



Nitrogen-doped graphene supported NiFe₂O₄ nanoparticles as high-performance anode material for lithium-ion batteries

Shugang Pan^{1,2,*}  and Xianmin Zhao^{2,*}

¹Changzhou Institute of Technology, Changzhou, China

²Nanjing University of Science and Technology, Nanjing, China

Received: 24 July 2021

Accepted: 18 September 2021

Published online:

28 September 2021

© The Author(s), under exclusive licence to Springer Science+Business Media, LLC, part of Springer Nature 2021

ABSTRACT

Nitrogen-doped graphene supported NiFe₂O₄ nanoparticles (NiFe₂O₄-NG) composite was successfully synthesized by a simple hydrothermal method. In the NiFe₂O₄-NG nanocomposite, the surface of nitrogen-doped graphene sheets was loaded by a large number of uniform NiFe₂O₄ nanoparticles with the mean size of 8 nm. Meanwhile, the nitrogen-doped graphene sheets were exfoliated. As anode materials for lithium ion batteries, the initial discharge and charging capacities of NiFe₂O₄-NG electrode are 1888 and 1242 mAh g⁻¹, respectively, and the coulomb efficiency is 65.8%. Furthermore, the capacity of NiFe₂O₄-NG is 1100 mAh g⁻¹ after 50 cycles. Compared with pure NiFe₂O₄, the superior electrochemical performance of the NiFe₂O₄-NG nanocomposite is mainly attributed to the unique architecture of smaller NiFe₂O₄ nanoparticles loaded on the high conductivity of nitrogen-doped graphene sheets, as well as the synergy effect between the nitrogen-doped graphene and nanoparticles. The high specific surface area of NiFe₂O₄-NG can increase the interface area between electrode and electrolyte, ensuring the full contact between electrode surface and electrolyte. The strong interaction between nitrogen-doped graphene and nanoparticle is beneficial to effectively suppress the volume expansion and the rapid ion/electron transport during the charge–discharge process. Profiting from structure and composition characteristics, the above-mentioned NiFe₂O₄-NG electrode delivers an excellent capacity, cycle performance and rate capability.

Address correspondence to E-mail: panshugang2010@163.com; zhaoxm@yandex.com

1 Introduction

With the increase of energy consumption and demand, more and more work is focused on the research of energy storage devices [1–4]. Among all kinds of energy storage devices, lithium-ion battery (LIB) is becoming the main battery technology because of its excellent characteristics [5, 6]. To a large extent, the performance of LIB mainly depends on the electrode active materials [7, 8]. Nowadays, graphite anode is the most commonly used, which cannot meet the urgent needs of hybrid electric vehicle (HEV) and electric vehicle (EV) with high energy and power density. Ferrite with high theoretical specific capacity and natural abundance has attracted great attention as the next generation of high-energy LIB anode materials [5, 9–17]. However, for a single ferrite electrode, its application is greatly limited due to poor conductivity, easy volume expansion and contraction in the process of charge and discharge, and the particles are easy to cluster and rupture. One of the most effective methods to improve ferrite anode materials is to form a composite of ferrite nanoparticles and carbon based materials to improve the electrochemical lithium storage performance of electrode materials. Among many carbon based materials [18–23], graphene has been widely studied as anode materials for LIB because of its large surface area, thermal conductivity and high conductivity, and excellent chemical stability. For example, the formation of ZnFe_2O_4 /graphene [24–29] binary nanocomposites greatly improves the cycle capacity of LIB. And according to the report [30–36], the way of doping heteroatoms can be significantly adjust electronic layer structure of graphene, which can improve the electrochemical performance of graphene. Among them, nitrogen (N) atom is the most widely introduced heteroatom. The lone electron pair of N atom can form delocalization conjugation system with sp^2 hybrid carbon skeleton, which effectively improves the conductivity graphene [30, 37–39]. In addition, for N-doped graphene materials, the introduction of N atoms can induce more defects and disordered surface morphology on graphene nanosheets, and the wetting effect between electrode and electrolyte is enhanced, which will be conducive to the improvement of lithium storage performance of electrode materials [40–45].

In view of the characteristics of the above materials, in this study, the raw material graphite oxide (GO) is prepared for standby; then, we simultaneously realized the reduction of GO, the N-doping process of graphene and uniformly loading of small-size NiFe_2O_4 nanoparticles with an average particle size of 8 nm on the surface of N-doped graphene (NG) through a simple one-step hydrothermal reaction. In the process of material preparation, the existence of NG can not only facilitate the formation and effective dispersion of NiFe_2O_4 nanoparticles, but also effectively inhibit the aggregation of formed small-size NiFe_2O_4 nanoparticles. Compared with pure NiFe_2O_4 , the NiFe_2O_4 -NG nanocomposite possesses a larger specific surface area, which is conducive to increasing the interface area between electrode and electrolyte and ensuring the full contact between electrode surface and electrolyte. At the same time, the strong interaction between NG and NiFe_2O_4 nanoparticles loaded on its surface is beneficial to effectively suppress the volume expansion and the rapid ion/electron transport during the charge–discharge process. Therefore, after the introduction of NG, NiFe_2O_4 -NG nanocomposites exhibit good capacity, cycle and rate performance such as the initial discharge and charging capacities of 1888 and 1242 mAh g^{-1} at 0.1 A g^{-1} , respectively, the coulomb efficiency of 65.8%, and the capacity of 1100 mAh g^{-1} after 50 cycles. Furthermore, the reversible cycle capacity of NiFe_2O_4 -NG can still reach 350 mAh g^{-1} when the current density reaches 1.0 A g^{-1} . This strategy provides a possible route to prepare high performance NG nanocomposite anodes and can be extended to other ferrite materials such as CoFe_2O_4 , ZnFe_2O_4 .

2 Experimental

2.1 Preparation of NiFe_2O_4 -NG nanocomposites

GO was fabricated according to the method reported by the researchers [46, 47]. Other reagents are analytical grade reagents purchased from Sinopharm Chemical Reagent Co., Ltd., and no further purification is required during use.

120 mg of GO was evenly dispersed into 120 mL of alcohol with sonication, and then 20 mL alcohol solution of $\text{Ni}(\text{NO}_3)_2 \cdot 6\text{H}_2\text{O}$ (0.5844 g) and

$\text{Fe}(\text{NO}_3)_3 \cdot 9\text{H}_2\text{O}$ (1.6220 g) was slowly added into the dispersion of GO under magnetic stirring for 0.5 h at room temperature. After that, 20 mL aqueous solution of urea (10 g) was dropped slowly added under magnetic stirring for 1 h. Finally, the obtained mixed solution was transferred to Teflon-lined stainless steel autoclave and placed in an oven at 180 °C for 20 h. The precipitate was washed with deionized water, freeze-dried, and then labeled as $\text{NiFe}_2\text{O}_4\text{-NG}$.

2.2 Characterization

The samples were characterized by powder X-ray diffraction (XRD) using a Bruker D8 Advance diffractometer with Cu K α radiation ($\lambda = 0.154178$ nm) in the angle range from 5 to 80°. The N_2 adsorption and desorption isotherms of the samples were determined by multi-channel automatic specific surface and pore analyzer of Micromeritics TriStar II 3020. Transmission electron microscopy (TEM) images were executed on a JEOL JEM2100 microscope. X-ray photoelectron spectra (XPS) were recorded on Thermo ESCALAB 250 system with Al K α irradiation ($h\nu = 1486.6$ eV).

2.3 Electrochemical measurements

Preparation of working electrode: working electrode is composed of active material, polyvinylidene fluoride, acetylene black (Super-P) and in the mass ratio of 8:1:1, and N-methyl-2-pyrrolidinone as the dispersion solvent to make an uniform slurry with certain viscosity. The mixed slurry is evenly coated on the copper foil with a diameter of 10 mm and dried in vacuum drying oven at 60 °C for more than 12 h. A self-made Swagelok half cell was assembled in a glove box filled with high purity argon shielding gas, using the prepared electrode sheet as working electrode and lithium metal sheet as counter electrode and reference electrode, 1 M LiPF_6 solution of ethylene carbonate (EC) and diethyl carbonate (DEC) ($V_{\text{EC}}/V_{\text{DEC}} = 1:1$) as electrolyte, polypropylene microporous membrane (Celgard 2400) as membrane. The instruments used for battery test are CHI660 electrochemical workstation and Land CT2001A charge discharge tester.

3 Results and discussion

The crystal microstructures and phase composition of GO, NG, pure NiFe_2O_4 and $\text{NiFe}_2\text{O}_4\text{-NG}$ were studied by XRD. As shown in Fig. 1, all XRD diffraction peaks of prepared NiFe_2O_4 are consistent with the standard card (JCPDS 54-0964). The diffraction peaks at 2θ values of 18.3°, 30.2°, 35.4°, 43.4°, 58.1° and 62.9° correspond to the (111), (220), (311), (400), (511) and (440) planes, respectively. There is no characteristic diffraction peak (001) of GO in the XRD diffraction pattern of $\text{NiFe}_2\text{O}_4\text{-NG}$, which is mainly due to the reduction of GO and the formation of NG by urea and solvent ethanol in the hydrothermal process. In addition, with the in-situ nucleation and growth of NiFe_2O_4 nanoparticles, the lamellar spacing of NG is further expanded, resulting in the disappearance of the (002) characteristic diffraction peak of NG. Moreover, it can be seen that the diffraction peaks of $\text{NiFe}_2\text{O}_4\text{-NG}$ nanocomposites become much weaker and wider more than those of pure NiFe_2O_4 nanoparticles, indicates that the addition of NG can effectively control the synthesis of NiFe_2O_4 particles with smaller particle size.

In order to better observe the microstructure and morphology of the $\text{NiFe}_2\text{O}_4\text{-NG}$ nanocomposites, SEM and TEM technology were applied. Figure 2a indicates that the surface of the NG was decorated with a large number of tiny NiFe_2O_4 particles through a simple hydrothermal method. As shown in Fig. 2b, it can be found that the NiFe_2O_4 particles in the $\text{NiFe}_2\text{O}_4\text{-NG}$ nanocomposites are very small (average particle size is about 8 nm) and uniformly

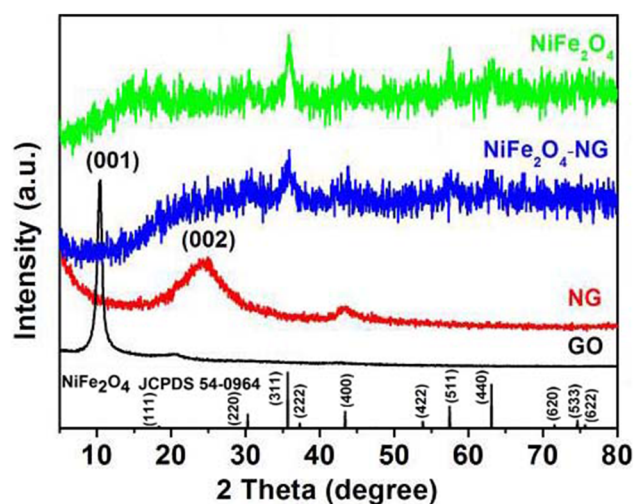


Fig. 1 XRD patterns of GO, NG, pure NiFe_2O_4 and $\text{NiFe}_2\text{O}_4\text{-NG}$

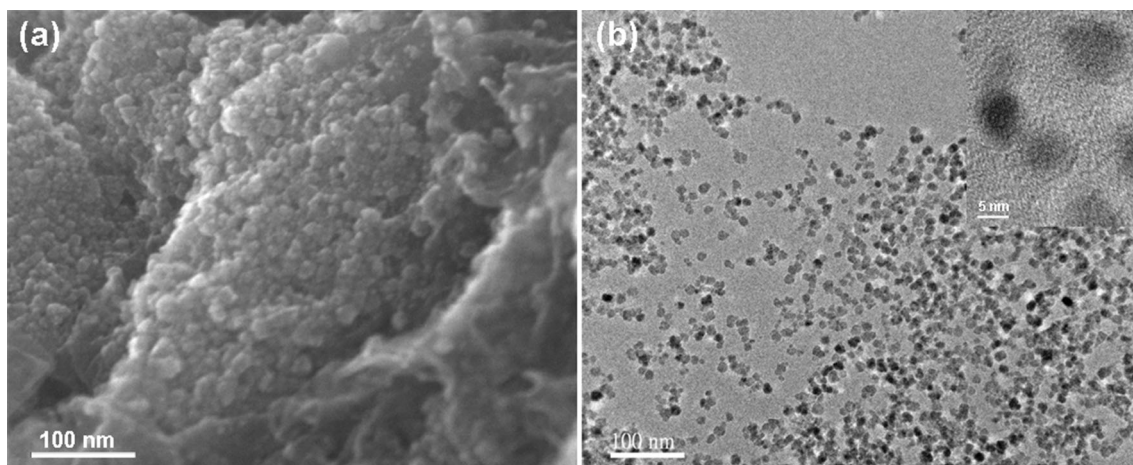


Fig. 2 **a** SEM image, **b** TEM image and HRTEM image (Inset) of NiFe₂O₄-NG

loaded on the surface of NG. Combining with the HRTEM image in Fig. 2b (Inset), the good dispersion of NiFe₂O₄ nanoparticles on NG surface can be more clearly observed in the NiFe₂O₄-NG nanocomposites. Thus, it can be inferred that NG as a good carbon based carrier can effectively avoid the agglomeration of nanoparticles and control the dispersion uniformity of nanoparticles on the surface of NG [7]. Due to the small particle size of the NiFe₂O₄-NG nanocomposites, the ion/electron transport path can be shortened, and the cycle stability and rate performance can be improved. In addition, almost all NiFe₂O₄ nanoparticles are tightly fixed to NG sheets and do not appear outside the NG sheets in the process of sample preparation by ultrasonication, suggesting there is a strong interaction between NiFe₂O₄ nanoparticles and NG. This strong interaction is beneficial to effectively suppress the volume expansion during the charge–discharge process [30]. All these merits may improve the lithium storage performance of the materials as anode materials for LIB.

Raman spectroscopy is a powerful technique to characterise the structure, especially to study the defects and disorder of carbon materials. As presented in Fig. 3, all of the materials (except pure NiFe₂O₄) have two remarkable peaks of carbon materials, which are assigned as D and G bands respectively. The D peak is caused by the lattice defects, and the G peak is on account of the stretching of all pairs of *sp*² atoms in both rings and chains [48]. For GO, Raman peaks of D-band and G-band are around 1342 cm⁻¹ and 1591 cm⁻¹, respectively. In addition, it can be found from Table 1 that the

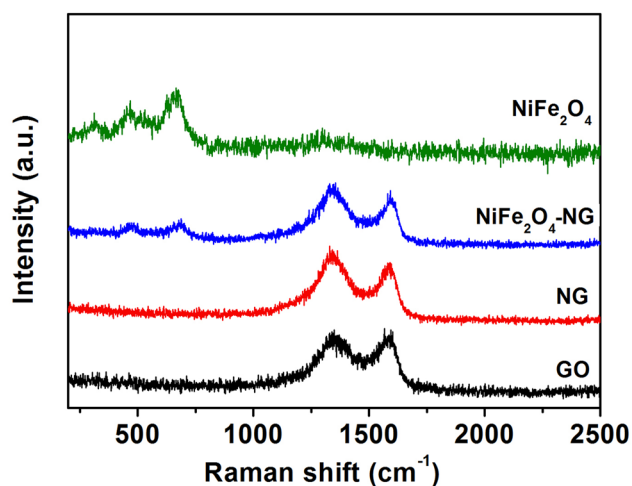


Fig. 3 Raman spectra of GO, NG, pure NiFe₂O₄, NiFe₂O₄-NG

Table 1 The value of I_D/I_G of GO, NG and NiFe₂O₄-NG

| Sample | GO | NG | NiFe ₂ O ₄ -NG |
|-----------|------|------|--------------------------------------|
| I_D/I_G | 0.97 | 1.16 | 1.22 |

intensity ratio of the D to G band (I_D/I_G) for GO is about 0.97. After reduction, Raman peaks of D-band corresponding to NG and NiFe₂O₄-NG appeared respectively at 1333 cm⁻¹ and 1336 cm⁻¹ (Fig. 3), and the ratio of I_D/I_G reached 1.16 and 1.22 accordingly (Table 1), indicative of a significant increase in structural and topological defects [48–50], especially for the NiFe₂O₄-NG nanocomposite.

XPS technology was applied to study and analyze the surface element composition and the valence state

of the as-obtained samples. C 1s core-level XPS spectra of NiFe₂O₄-NG in Fig. 4a could be deconvoluted into four peaks at 284.8, 285.9, 287.1 and 289 eV, which are assigned to the C=C, C-N, C-O-C and O-C=O, respectively [51]. Comparing the C 1s spectra of GO [52] (our previous work) and reduced GO (RGO) (Fig. 4a), the presence of C-N bond in the NiFe₂O₄-NG nanocomposite demonstrates the successful doping of N atoms. Simultaneously, the C 1s XPS peaks of oxygen-containing bonds shift obviously, indicating that there is a strong interaction between NiFe₂O₄ and NG [30], which can provide the rapid transfer channels for electrons and ions, and thus improving the charge/discharge performance of NiFe₂O₄-NG. Combining with the high-resolution spectra for N 1s of NiFe₂O₄-NG nanocomposites, the N doping can be further confirmed. In Fig. 4b of N 1s XPS spectra for NiFe₂O₄-NG nanocomposites, the peaks at 398.8, 400.1 and 401.4 eV are attributed to N atoms of pyridine type, pyrrole type and graphite

phase, respectively, which further proved that N atoms were successfully doped into graphene in NiFe₂O₄-NG nanocomposites [1]. It is worth noting that pyridinic N and pyrrolic N are the main chemical states of introduced N atoms, which can be as active sites for the assembling of metal nanoparticles, enhancing the electrochemical activity of electrode materials [53–55]. In addition, the two characteristic peaks locate at 710.8 eV and 724.5 eV are corresponded to Fe 2p_{3/2} and Fe 2p_{1/2} (Fig. 4c), respectively, which can be attributed to the existence of Fe³⁺ [56–58]. The Ni 2p spectra in Fig. 4d showed two peaks of 2p_{3/2} and 2p_{1/2}, located at 854.9 and 872.6 eV, respectively [58], accompanying two satellite peaks.

Figure 5 shows the nitrogen adsorption/desorption isotherms of NG and NiFe₂O₄-NG nanocomposites. It can be seen that the isotherms of the above materials are type IV. Based on the fitting analysis of BET equation, the BET surface areas of NG and

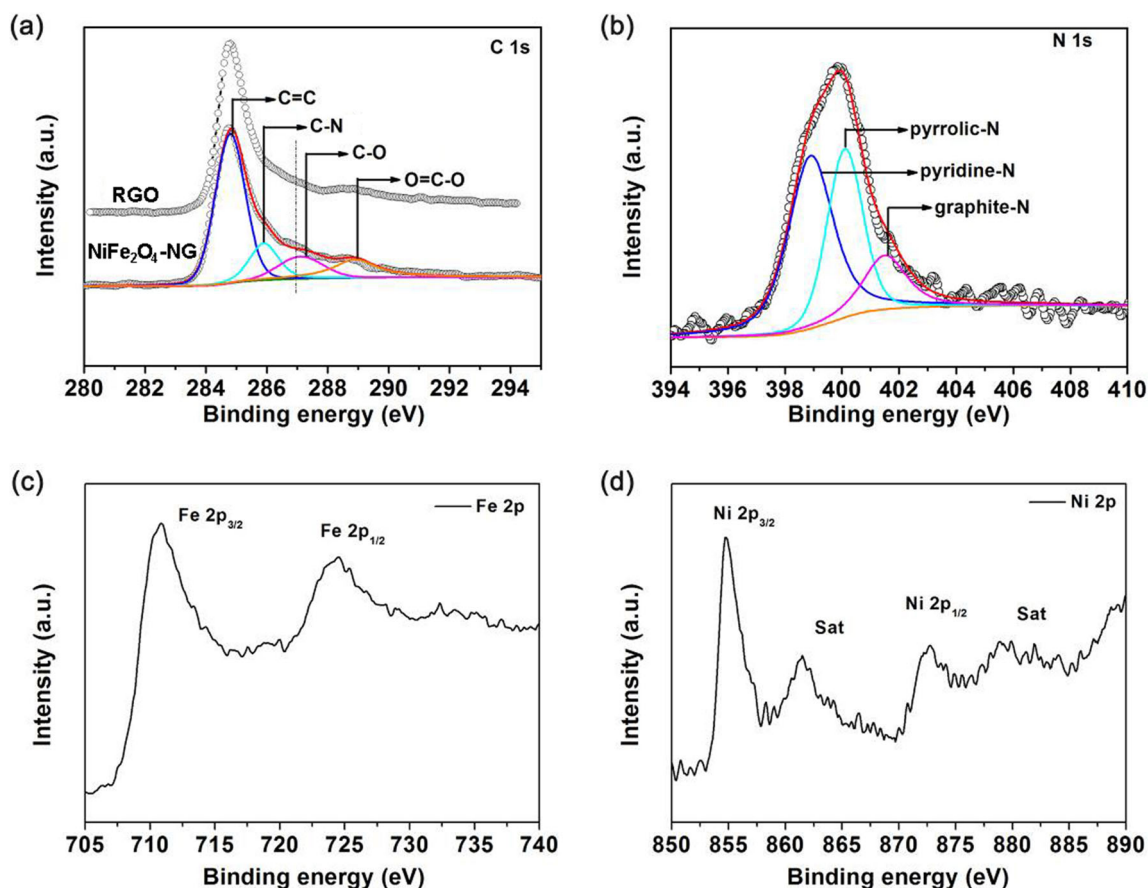


Fig. 4 a C 1s core-level XPS spectra of reduced graphite oxide (RGO) and NiFe₂O₄-NG; b N 1s; c Fe 2p; d Ni 2p core-level XPS spectra of NiFe₂O₄-NG

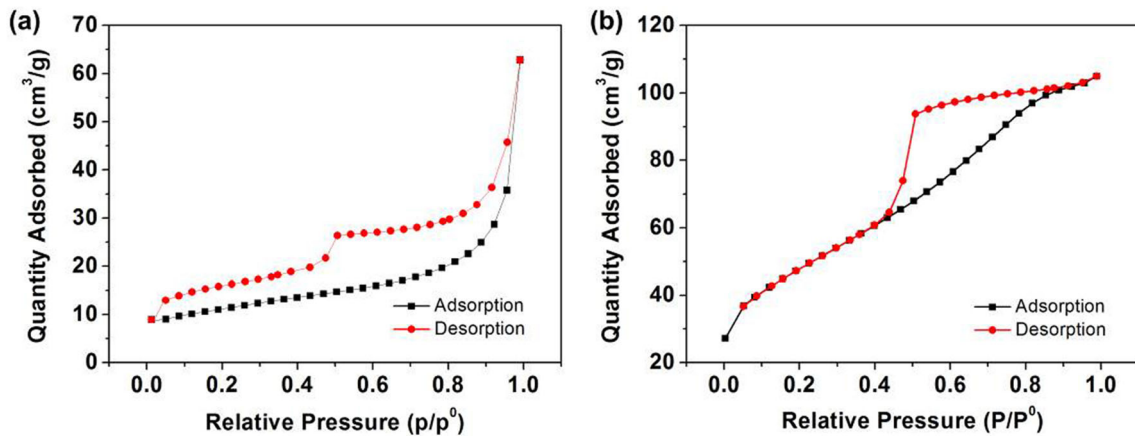


Fig. 5 Nitrogen adsorption/desorption isotherm of **a** NG, **b** NiFe₂O₄-NG

NiFe₂O₄-NG are estimated to be 38.3 m² g⁻¹ and 167.8 m² g⁻¹, respectively. The large surface areas of NiFe₂O₄-NG may be ascribed to the fact that the NG lamellar structure can inhibit the agglomeration of nanoparticles when uniformly loaded with NiFe₂O₄ nanoparticles. On the other hand, the existence of nanoparticles inhibits the secondary stacking of NG nano layer, which greatly improves the specific surface area of the composites. In this way, the high specific surface area of NiFe₂O₄-NG can increase the interface area between electrode and electrolyte, ensure the full contact between electrode surface and electrolyte, therefore improving its electrochemical performance [23, 31, 40].

The electrochemical properties of pure NiFe₂O₄ and NiFe₂O₄-NG nanocomposites electrode materials were investigated by constant current charge/discharge test. In Fig. 6a, for pure NiFe₂O₄, the voltage plateau respectively appears at about 0.75 V and

1.7 V during the first charge and discharge, corresponding to the reduction and oxidation reaction on the electrode during lithium ion insertion and desorption [3, 11]. The first discharge capacity and charging capacity of pure NiFe₂O₄ are 1449 and 629 mAh g⁻¹, respectively, and the corresponding coulomb efficiency is 43.4% (Fig. 8). The capacity loss of the first charge/discharge is mainly attributed to the occurrence of irreversible reaction and the formation of solid electrolyte membrane (SEI) [59–61]. With the charge and discharge process, the coulomb efficiency increases, the voltage plateau becomes shorter, and the capacity decreases sharply. Furthermore, the capacity of pure NiFe₂O₄ is only 80 mAh g⁻¹ after 50 cycles, which is mainly due to the embedding/disembedding of lithium ions. This makes the structure of pure NiFe₂O₄ unable to withstand the volume shrinkage and expansion, resulting in poor cycle stability. Compared with pure NiFe₂O₄, the initial

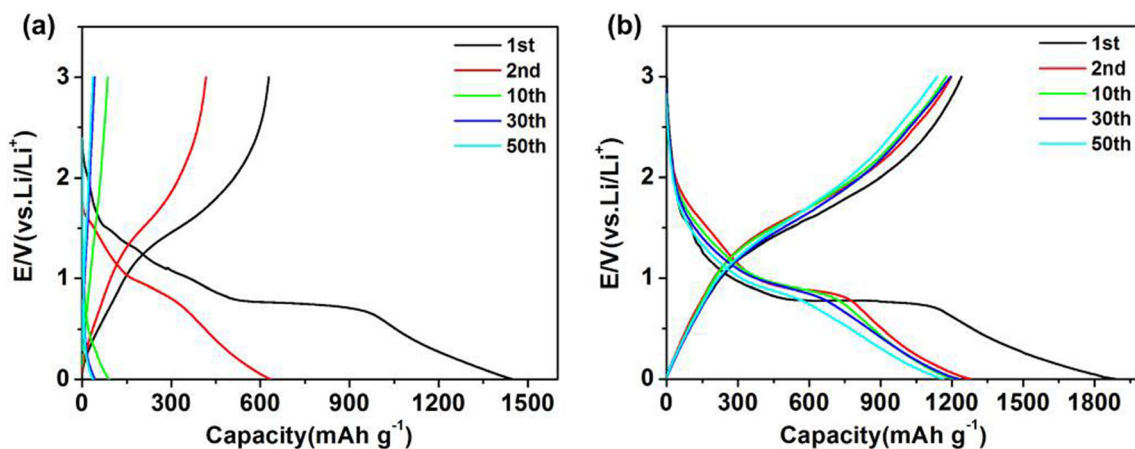


Fig. 6 Charge/discharge curves of **a** pure NiFe₂O₄, **b** NiFe₂O₄-NG. (Current density is 100 mA g⁻¹)

discharge and charging capacities of NiFe₂O₄-NG (Fig. 6b) electrode are 1888 mAh g⁻¹ and 1242 mAh g⁻¹, respectively, and the coulomb efficiency is 65.8% (Fig. 8), indicating that the introduction of NG largely inhibits the occurrence of irreversible reaction. Moreover, the capacity of NiFe₂O₄-NG is 1100 mAh g⁻¹ after 50 cycles. The excellent lithium storage performance of NiFe₂O₄-NG nanocomposite materials is mainly due to the following reasons: the addition of NG can effectively control the growth of NiFe₂O₄ nanoparticles, enduing the nanoparticles with uniform dispersion on the surface of NG nanosheets, further leading to a larger specific surface area, alleviating the volume change in the process of multiple charge and discharge [9]. In addition, the strong contact and interaction between NiFe₂O₄ nanoparticles and NG nanosheets, the excellent charge transport and structural stability of NiFe₂O₄-NG nanocomposites are also important factors to improve the electrochemical performance [7].

Figure 7 shows the cyclic voltammetry curves of pure NiFe₂O₄ and NiFe₂O₄-NG nanocomposites electrode materials at a current density of 100 mA g⁻¹ and a voltage range of 0.01–3 V. For pure NiFe₂O₄ electrode (Fig. 7a), there is an obvious cathodic reduction peak at 0.41 V, corresponding to the reduction of Ni²⁺ and Fe³⁺ to Ni and Fe, and the intercalation of lithium ions. The anodic oxidation peak appeared at 1.87 V, mainly due to the oxidation process of Ni⁰ to Ni²⁺ and Fe⁰ to Fe²⁺. Compared with the first cycle, the redox peak intensity of the second cycle decreased and shifted, causing by the formation of SEI film and the occurrence of irreversible reaction during the first cycle [11, 13, 14], which was consistent with the above results of charge discharge curve. In addition, the reduction peak cracks into two peaks because the structure of NiFe₂O₄ is destroyed during the charging and discharging process. With the addition of NG (Fig. 7b), the reduction peak still appears at about 0.4 V, corresponding to the reduction of Ni²⁺ and Fe³⁺. Accordingly, the oxidation peak of metal appears at 1.87 V. Moreover, with the increase of the number of cycles, the reduction peak and oxidation peak shift to 0.67 V and 1.94 V, respectively. Furthermore, compared with Fig. 7a and b, it is obvious that the CV curves of NiFe₂O₄-NG nearly overlap in the second and third cycles, which suggests that the addition of NG can effectively improve the cycle stability.

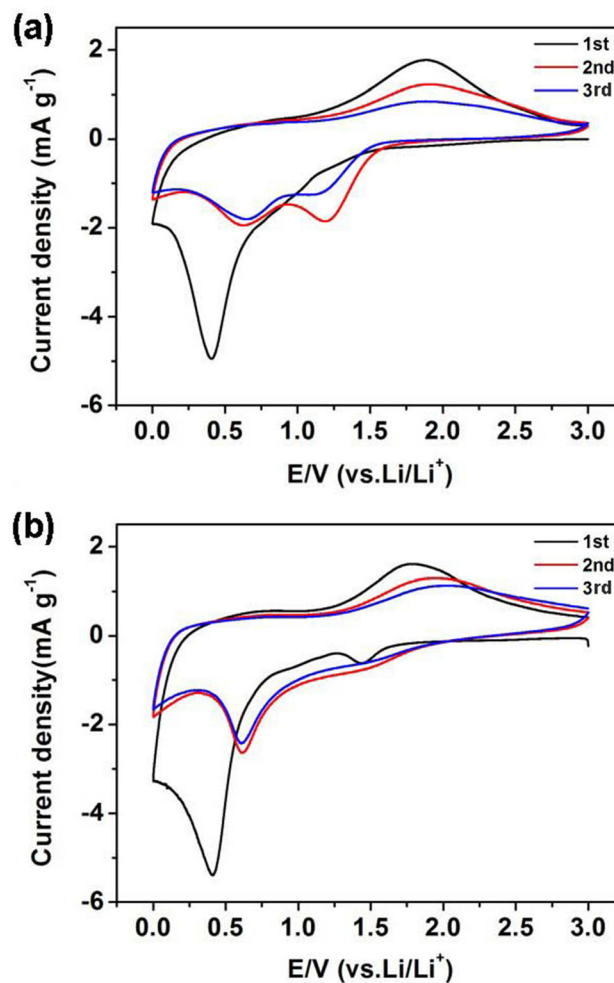
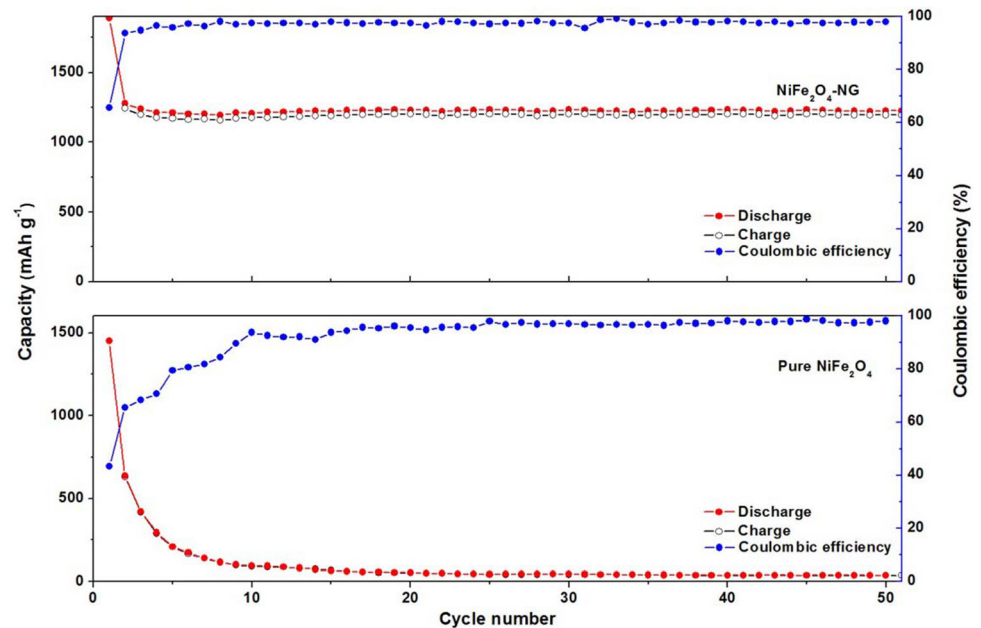


Fig. 7 Cyclic voltammograms of **a** pure NiFe₂O₄, **b** NiFe₂O₄-NG at a sweep rate of 1 mV s⁻¹

In order to better reflect the change of lithium storage capacity of electrode materials in the process of multiple charge and discharge, cycle performance of pure NiFe₂O₄ and NiFe₂O₄-NG electrode is studied and shown in Fig. 8. It can be seen that the specific capacity of pure NiFe₂O₄ electrode decreases sharply with the increase of cycle number. The cycle performance of NiFe₂O₄-NG electrode is significantly improved after compounding with NG. Furthermore, the specific capacity of NiFe₂O₄-NG electrode is still 1100 mAh g⁻¹ after 50 cycles, and the capacity retention rate is more than 90%. This is mainly due to the addition of NG, which ensures the stability of nanoparticle structure in the process of charge and discharge. At the same time, the strong contact and interaction between NiFe₂O₄ nanoparticles and NG nanosheets, the excellent charge transport and structural stability of NiFe₂O₄-NG nanocomposites,

Fig. 8 Cycling performance of **a** pure NiFe₂O₄, **b** NiFe₂O₄-NG. (Current density is 100 mA g⁻¹)



better synergistically contribute the excellent electrochemical performance of electrode materials.

The electrochemical properties of pure NiFe₂O₄ and NiFe₂O₄-NG nanocomposite electrode materials were further studied by rate performance test at a voltage range of 0.01–3 V and the results are displayed in Fig. 9a. When the current density are 0.1 A g⁻¹, 0.2 A g⁻¹, 0.3 A g⁻¹ and 0.5 A g⁻¹, the reversible cycle capacities of NiFe₂O₄-NG are 1100, 1000, 900, 650 mAh g⁻¹, respectively. Even the current density reaches 1.0 A g⁻¹, the reversible cycle capacity of NiFe₂O₄-NG can still reach 350 mAh g⁻¹. Furthermore, when the current density returns to 0.1 A g⁻¹, the reversible capacity can still be up to 1000 mAh g⁻¹, showing excellent high current charge/discharge performance, which can be attributed to the formation of smaller NiFe₂O₄ nanoparticles and the high conductivity of NG sheets. The electrochemical impedance spectra (EIS) of pure NiFe₂O₄, NiFe₂O₄-NG nanocomposites were measured. It can be seen from Fig. 9b that the EIS curves of both pure NiFe₂O₄ and NiFe₂O₄-NG nanocomposites electrodes are composed of semicircles in high frequency region and oblique lines in low frequency region. The semicircle represents the charge transfer reaction between the electrode and the electrolyte interface, and the oblique line reflects the lithium ion diffusion process [62, 63]. The diameter of half arc in high frequency region of NiFe₂O₄-NG electrode is much smaller than that of pure NiFe₂O₄ electrode, which

indicates that NiFe₂O₄-NG electrode has low interface contact, mass transfer resistance and good electron transmission capability [30]. In order to better observe the electrochemical performance, the diffusion coefficient (*D*) of lithium ion is analyzed in the low frequency region according to the following equation [64, 65]:

$$D = \frac{R^2 T^2}{2C^2 A^2 F^4 n^4 \sigma^2} \quad (1)$$

$$Z_W = R_D + R_L + \sigma \omega^{-1/2} \quad (2)$$

where *R* is the gas constant, *T* is the absolute temperature, *C* is the initial concentration in mol cm⁻³, *F* is the Faraday constant, *n* is the number of electrons per molecule during oxidization, and σ is the Warburg factor which is relative to *Z_W* [seen in Eq. (2)]. Concurrently, the relationship between the *Z_W* and the square root of frequency ($\omega^{-1/2}$) in the low frequency region is shown in Fig. 9c. Due to the low content of NG, the *C* value of the pure NiFe₂O₄ and NiFe₂O₄-NG electrodes are approximately equal. So, the ratio (*K*) of *D_{NiFe₂O₄-NG}* to *D_{NiFe₂O₄}* can be calculated by the following Eq. (3):

$$K = \frac{D_{\text{NiFe}_2\text{O}_4\text{-NG}}}{D_{\text{NiFe}_2\text{O}_4}} \approx \frac{\sigma_{\text{NiFe}_2\text{O}_4}^2}{\sigma_{\text{NiFe}_2\text{O}_4\text{-NG}}^2} \quad (3)$$

Combining the Nyquist diagram in the low frequency region (Fig. 9b) and Eq. (2), the slope of the line in Fig. 9c is the value of σ . Therefore, the value of

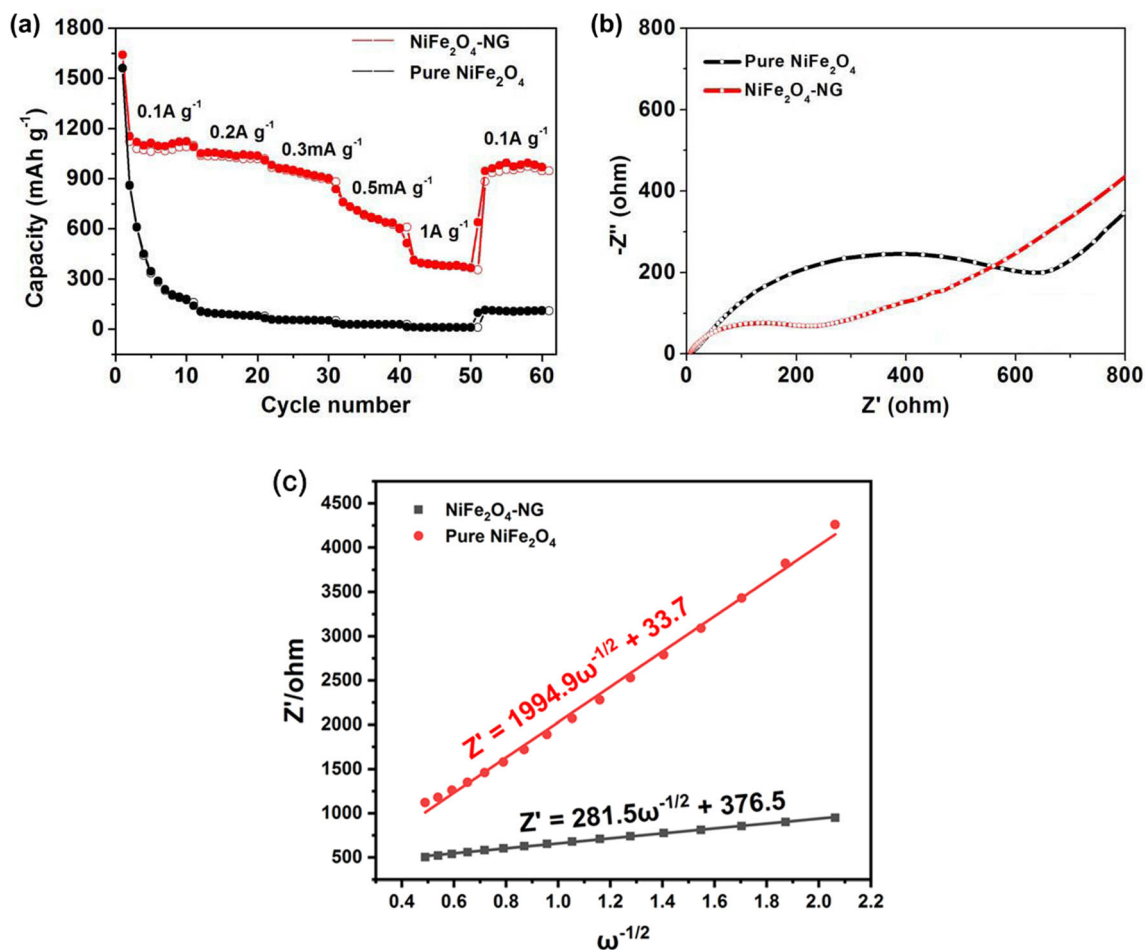


Fig. 9 **a** Rate performance at various current density; **b** Electrochemical impedance spectroscopy (EIS); **c** the relationship between Z' and $\omega^{-1/2}$ in the low-frequency region of pure NiFe_2O_4 and $\text{NiFe}_2\text{O}_4\text{-NG}$

σ of the pure NiFe_2O_4 and $\text{NiFe}_2\text{O}_4\text{-NG}$ electrodes are 1994.9 and 281.5, respectively. Thus, it can be calculated that the K value is 50.2 by Eq. (3). The above results better illustrate that $\text{NiFe}_2\text{O}_4\text{-NG}$ electrode possesses superior lithium-ion intercalation/de-intercalation kinetics, resulting in a significant amelioration in rate capability.

Based on the above experimental data and results, the superior lithium storage performance of $\text{NiFe}_2\text{O}_4\text{-NG}$ electrode mainly come from the following aspects. Firstly, a large number of uniformly dispersed and small NiFe_2O_4 nanoparticles on the surface of NG can shorten the ion/electron transmission path, which are beneficial for the improvement of cycle stability and rate performance. Secondly, the large surface areas and the strong interaction between NiFe_2O_4 nanoparticles and NG nanosheets in $\text{NiFe}_2\text{O}_4\text{-NG}$ electrode can not only increase the interface area between electrode and electrolyte, but

also alleviate the volume change in the process of multiple charge and discharge, which is conducive to the full contact between electrode surface and electrolyte and the enhancement of the stability of nanoparticle structure in the process of charge and discharge, resulting in an enhanced cycling stability. Finally, the high diffusion coefficient of lithium ion in $\text{NiFe}_2\text{O}_4\text{-NG}$ electrode implies that it has superior lithium-ion intercalation/de-intercalation kinetics, consequently resulting in an enhanced rate capability.

4 Conclusions

In summary, $\text{NiFe}_2\text{O}_4\text{-NG}$ nanocomposites were successfully obtained using NG sheets as a support material by a simple hydrothermal reaction. In the whole reaction process, the NiFe_2O_4 nanoparticles

with the mean size of 8 nm were uniformly loaded on the surface of NG sheets. As anode materials for LIB, the initial discharge and charging capacities of NiFe₂O₄-NG electrode are 1888 and 1242 mAh g⁻¹, respectively, and the coulomb efficiency is 65.8%. Moreover, the capacity of NiFe₂O₄-NG is 1100 mAh g⁻¹ after 50 cycles. Compared with pure NiFe₂O₄, the NiFe₂O₄-NG nanocomposites delivered superior electrochemical performance because of the structure formation of smaller NiFe₂O₄ nanoparticles loaded on the high conductivity of NG sheets. The high specific surface area of NiFe₂O₄-NG can increase the interface area between electrode and electrolyte, ensure the full contact between electrode surface and electrolyte. The strong interaction between NG and nanoparticles is beneficial to effectively suppress the volume expansion and the rapid ion/electron transport during the charge–discharge process.

Acknowledgements

This work was supported by Changzhou Sci & Tech Program (Grant No. CJ20190011).

References

1. R. Yadav, C.K. Dixit, Characterization and prospective applications of nitrogen-doped graphene. *J. Sci.-Adv. Mater. Dev.* **2**, 141–149 (2017)
2. S.Y. Lee, C.H. Choi, M.W. Chung, J.H. Chung, S.I. Woo, Dimensional tailoring of nitrogen-doped graphene for high performance supercapacitors. *RSC Adv.* **6**, 55577–55583 (2016)
3. Y.G. Guo, J.S. Hu, L.J. Wan, Nanostructured materials for electrochemical energy conversion and storage devices. *Adv. Mater.* **20**, 2878–2887 (2008)
4. J.C. Shearer, A. Cherevan, D. Eder, Application and future challenges of functional nanocarbon hybrids. *Adv. Mater.* **26**, 2295–2318 (2014)
5. X.X. Liu, E. Liu, D.L. Chao, L. Chen, S. Liu, J. Wang, Y. Li, J.P. Zhao, Y.M. Kang, Z.X. Shen, Large size nitrogen-doped graphene-coated graphite for high performance lithium-ion battery anode. *RSC Adv.* **6**, 104010–104015 (2016)
6. B. Xiang, W.L. An, J.J. Fu, S.X. Mei, S.G. Guo, X.M. Zhang, B. Gao, P.K. Chu, Graphene-encapsulated blackberry-like porous silicon nanospheres prepared by modest magnesiothermic reduction for high-performance lithium-ion battery anode. *Rare Met.* **40**, 383–392 (2021)
7. Y.K. Zhou, J.M. Lu, C.J. Deng, H.X. Zhu, G.Z. Chen, S.W. Zhang, X.H. Tian, Nitrogen-doped graphene guided formation of monodisperse microspheres of LiFePO₄ nanoplates as the positive electrode material of lithium-ion batteries. *J. Mater. Chem. A* **4**, 12065–12072 (2016)
8. T.J. Wu, M.J. Jing, Y. Tian, L. Yang, J.G. Hu, X.Y. Cao, G.Q. Zou, H.S. Hou, X.B. Ji, Surface-driven energy storage behavior of dual-heteroatoms functionalized carbon material. *Adv. Funct. Mater.* **29**, 1900941 (2019)
9. A.K. Rai, L.T. Anh, J. Gim, V. Mathew, J. Kang, B.J. Paul, N.K. Singh, Facile approach to synthesize CuO/reduced graphene oxide nanocomposite as anode materials for lithium-ion battery. *J. Power Sources* **244**, 435–441 (2013)
10. M.Y. Zhu, X. Zhang, Y. Zhou, C.H. Zhuo, J.C. Huang, S.J. Li, Facile solvothermal synthesis of porous ZnFe₂O₄ microspheres for capacitive pseudocapacitors. *RSC Adv.* **5**, 39270–39277 (2015)
11. C. Vidal-Abarca, P. Lavela, J.L. Tirado, The origin of capacity fading in NiFe₂O₄ conversion electrodes for lithium ion batteries unfolded by Fe-57 Mossbauer spectroscopy. *J. Phys. Chem. C* **114**, 12828–12832 (2010)
12. K.V. Sankar, R.K. Selvan, D. Meyrick, Electrochemical performances of CoFe₂O₄ nanoparticles and a rGO based asymmetric supercapacitor. *RSC Adv.* **5**, 99959–99967 (2015)
13. L.H. Zhang, T. Wei, Z.M. Jiang, C.Q. Liu, H. Jiang, J. Chang, L.Z. Sheng, Q.H. Zhou, L.B. Yuan, Z.J. Fan, Electrostatic interaction in electrospun nanofibers: double-layer carbon protection of CoFe₂O₄ nanosheets enabling ultralong-life and ultrahigh-rate lithium ion storage. *Nano Energy* **48**, 238–247 (2018)
14. C.T. Cherian, J. Sundaramurthy, M.V. Reddy, P.S. Kumar, K. Mani, D. Pliszka, C.H. Sow, S. Ramakrishna, B.V. Chowdari, Morphologically robust NiFe₂O₄ nanofibers as high capacity Li-ion battery anode material. *ACS Appl. Mater. Interfaces* **5**, 9957–9963 (2013)
15. H. Xia, Y.Y. Qian, Y.S. Fu, X. Wang, Graphene anchored with ZnFe₂O₄ nanoparticles as a high-capacity anode material for lithium-ion batteries. *Solid State Sci.* **17**, 67–71 (2013)
16. Y.J. Yao, Z.H. Yang, D.W. Zhang, W.C. Peng, H.Q. Sun, S.B. Wang, Magnetic CoFe₂O₄-graphene hybrids: facile synthesis, characterization, and catalytic properties. *Ind. Eng. Chem. Res.* **51**, 6044–6051 (2012)
17. Y.S. Fu, Y.H. Wan, H. Xia, X. Wang, Nickel ferrite-graphene heteroarchitectures: toward high-performance anode materials for lithium-ion batteries. *J. Power Sources* **213**, 338–342 (2012)
18. X.X. Liu, D.L. Chao, Y. Li, J. Hao, X.S. Liu, J.P. Zhao, J.Y. Lin, H.J. Fan, Z.X. Shen, A low-cost and one-step synthesis of N-doped monolithic quasi-graphene films with porous

- carbon frameworks for Li-ion batteries. *Nano Energy* **17**, 43–51 (2015)
19. X.Y. Wang, F. Ling, D.C. Gong, J. Zh, Core-shell Ge@graphene@TiO₂ nanofibers as a high-capacity and cycle-stable anode for lithium and sodium ion battery. *Adv. Funct. Mater.* **26**, 1104–1111 (2016)
 20. D. Usachov, O. Vilkov, A. Grüneis, D. Haberer, A. Fedorov, V.K. Adamchuk, A.B. Preobrajenski, P. Dudin, A. Barinov, M. Oehzelt, C. Laubschat, D.V. Vyalikh, *Nano Lett.* **11**, 5401–5407 (2011)
 21. M.D. Stoller, S. Park, Y.W. Zhu, J.H. An, R.S. Ruoff, Graphene-based ultracapacitors. *Nano Lett.* **8**, 3498–3502 (2008)
 22. A.A. Balandin, S. Ghosh, W.Z. Bao, I. Calizo, D. Teweldebrhan, F. Miao, C.N. Lau, Superior thermal conductivity of single-layer graphene. *Nano Lett.* **8**, 902–907 (2008)
 23. Y.K. Zhou, J. Wang, Y.Y. Hu, R. O'Hayre, Z.P. Shao, A porous LiFePO₄ and carbon nanotube composite. *Chem. Commun.* **46**, 7151–7153 (2010)
 24. W.T. Song, J. Xie, S.Y. Liu, G.S. Cao, T.J. Zhu, X.B. Zhao, Self-assembly of a ZnFe₂O₄/graphene hybrid and its application as a high-performance anode material for Li-ion batteries. *New. J. Chem.* **36**, 2236–2241 (2012)
 25. J. Xie, W.T. Song, G.S. Cao, T.J. Zhu, X.B. Zhao, S.C. Zhang, One-pot synthesis of ultrafine ZnFe₂O₄ nanocrystals anchored on graphene for high-performance Li and Li-ion batteries. *RSC Adv.* **4**, 7703–7709 (2014)
 26. A.K. Rai, S.J. Kim, J. Gim, M.H. Alfaruqi, V. Mathew, J. Kim, Electrochemical lithium storage of a ZnFe₂O₄/graphene nanocomposite as an anode material for rechargeable lithium ion batteries. *RSC Adv.* **4**, 47087–47095 (2014)
 27. B. Wang, S.M. Li, B. Li, J.H. Liu, M. Yu, Facile and large-scale fabrication of hierarchical ZnFe₂O₄/graphene hybrid films as advanced binder-free anodes for lithium-ion batteries. *New J. Chem.* **39**, 1725–1733 (2015)
 28. Z. Li, J.H. Cao, Z.G. Xia, J.J. Zhang, M.Q. Fan, D.H. Wei, H. Yang, Self-assembled ZnFe₂O₄ hollow spheres/GO hybrid anode with excellent electrochemical performance for lithium-ion batteries. *J. Mater. Sci.* **31**, 1126–1134 (2020)
 29. Y. Park, M. Oh, J.H. Kim, Well-dispersed ZnFe₂O₄ nanoparticles onto graphene as superior anode materials for lithium ion batteries. *Energies* **12**, 304–318 (2019)
 30. X.Y. Jiao, L. Cai, X.F. Xia, W. Lei, Q.L. Hao, D. Mandler, Novel spinel nanocomposites of Ni_xCo_{1-x}Fe₂O₄ nanoparticles with N-doped graphene for lithium ion batteries. *Appl. Surf. Sci.* **481**, 200–208 (2019)
 31. C.M. Doherty, R.A. Caruso, C.J. Drummond, High performance LiFePO₄ electrode materials: influence of colloidal particle morphology and porosity on lithium-ion battery power capability. *Energy Environ. Sci.* **3**, 813–823 (2010)
 32. A. Ambrosi, H.L. Poh, L. Wang, Z. Sofer, M. Pumera, Capacitance of p- and n-doped graphenes is dominated by structural defects regardless of the dopant type. *ChemSuschem* **7**, 1102–1106 (2014)
 33. P. Ayala, R. Arenal, M.H. Rummeli, A. Rubio, T. Pichler, The doping of carbon nanotubes with nitrogen and their potential applications. *Carbon* **48**, 575–586 (2010)
 34. J.P. Paraknowitsch, A. Thomas, Doping carbons beyond nitrogen: an overview of advanced heteroatom doped carbons with boron, sulphur and phosphorus for energy applications. *Energy Environ. Sci.* **6**, 2839–2855 (2013)
 35. W.S.V. Lee, M. Leng, M. Li, X.L. Huang, J.M. Xue, Sulphur-functionalized graphene towards high performance supercapacitor. *Nano Energy* **12**, 250–257 (2015)
 36. H.L. Guo, P. Su, X.F. Kang, S.K. Ning, Synthesis and characterization of nitrogen-doped graphene hydrogels by hydrothermal route with urea as reducing-doping agents. *J. Mater. Chem. A* **1**, 2248–2255 (2013)
 37. E.H. Ahlgren, J. Kotakoski, A.V. Krashennnikov, Atomistic simulations of the implantation of low-energy boron and nitrogen ions into graphene. *Phys. Rev. B* **83**, 115424–115431 (2011)
 38. Z. Jin, J. Yao, C. Kittrell, J.M. Tour, Large-scale growth and characterizations of nitrogen-doped monolayer graphene sheets. *ACS Nano* **5**, 4112–4117 (2011)
 39. Y. Wang, Y.Y. Shao, D.W. Matson, J.H. Li, Y.H. Lin, Nitrogen-doped graphene and its application in electrochemical biosensing. *ACS Nano* **4**, 1790–1798 (2010)
 40. B. Wang, W.A. Abdulla, D.L. Wang, X.S. Zhao, A three-dimensional porous LiFePO₄ cathode material modified with a nitrogen-doped graphene aerogel for high-power lithium ion batteries. *Energy Environ. Sci.* **8**, 869–875 (2015)
 41. B. Wang, B.H. Xu, T.F. Liu, P. Liu, C.F. Guo, S. Wang, Q.M. Wang, Z.G. Xiong, D.L. Wang, X.S. Zhao, Mesoporous carbon-coated LiFePO₄ nanocrystals co-modified with graphene and Mg²⁺ doping as superior cathode materials for lithium ion batteries. *Nanoscale* **6**, 986–995 (2014)
 42. T.J. Wu, M.J. Jing, Y. Liu, X.B. Ji, Binding low crystalline MoS₂ nanoflakes on nitrogen-doped carbon nanotube: towards high-rate lithium and sodium storage. *J. Mater. Chem. A* **7**, 6439–6449 (2019)
 43. S. Yoon, C. Liao, X.G. Sun, C.A. Bridges, R.R. Unocic, J. Nanda, S. Dai, M.P. Paranthaman, Conductive surface modification of LiFePO₄ with nitrogen doped carbon layers for lithium-ion batteries. *J. Mater. Chem.* **22**, 4611–4614 (2012)
 44. X.J. Tan, C.F. Cui, S.Q. Wu, B.C. Qiu, L.Z. Wang, J.L. Zhang, Nitrogen-doped mesoporous carbon-encapsulated MoO₂ nanobelts as a high-capacity and stable host for lithium-ion storage. *Chem. Asian J.* **12**, 36–40 (2016)

45. J.J. Wang, X.L. Sun, Olivine LiFePO₄: the remaining challenges for future energy storage. *Energy Environ. Sci.* **8**, 1110–1138 (2015)
46. L.J. Cote, F. Kim, J.X. Huang, Langmuir–Blodgett assembly of graphite oxide single layers. *J. Am. Chem. Soc.* **131**, 1043–1049 (2009)
47. Y.L. Guo, C.A. Di, H.T. Liu, J. Zheng, L. Zhang, G. Yu, Y.Q. Liu, General route toward patterning of graphene oxide by a combination of wettability modulation and spin-coating. *ACS Nano* **10**, 5749–5754 (2010)
48. P. Peng, H.T. Liu, B. Wu, Q.X. Tang, Y.Q. Liu, Nitrogen doped graphene with a p-type field-effect and its fine modulation. *Acta Phys. Chim. Sin.* **35**, 1282–1290 (2019)
49. X. Díez-Betriu, S. Álvarez-García, C. Botas, P. Álvarez, J. Sánchez-Marcos, C. Prieto, R. Menéndez, A. Andrés, Raman spectroscopy for the study of reduction mechanisms and optimization of conductivity in graphene oxide thin films. *J. Mater. Chem. C* **1**, 6905–6912 (2013)
50. Y.Y. Wang, Z.W. Zhao, Y. Liu, L.R. Hou, C.Z. Yuan, Precipitant-free solvothermal construction of spindle-like CoCO₃/reduced graphene oxide hybrid anode toward high-performance lithium-ion batteries. *Rare Metal* **39**, 1082–1091 (2020)
51. Y.K. Zhou, J.M. Lu, C.J. Deng, H.X. Zhu, G.Z. Chen, S.W. Zhang, X.H. Tian, Nitrogen-doped graphene guided formation of monodisperse microspheres of LiFePO₄ nanoplates as the positive electrode material of lithium-ion batteries. *J. Mater. Chem. A* **31**, 12065–12072 (2016)
52. S.G. Pan, X.H. Liu, CdS-Graphene nanocomposite: synthesis, adsorption kinetics and high photocatalytic performance under visible light irradiation. *New J. Chem.* **36**, 1781–1787 (2012)
53. W.J. Wang, Q.L. Hao, W. Lei, X.F. Xia, X. Wang, Ternary nitrogen-doped graphene/nickel ferrite/polyaniline nanocomposites for high-performance supercapacitors. *J. Power Sources* **269**, 250–259 (2014)
54. S. Stankovich, D.A. Dikin, R.D. Piner, K.A. Kohlhaas, A. Kleinhammes, Y.Y. Jia, Y. Wu, S.T. Nguyen, R.S. Ruoff, Synthesis of graphene-based nanosheets via chemical reduction of exfoliated graphite oxide. *Carbon* **45**, 1558–1565 (2007)
55. W. Lei, W.M. Si, Q.L. Hao, Z. Han, Y.H. Zhang, M.Z. Xia, Nitrogen-doped graphene modified electrode for nimodipine sensing. *Sens. Actuators B* **212**, 207–213 (2015)
56. M. Choi, S.H. Lee, Y. Jung, J. Jung, J. Park, W. Choi, S. Park, H.J. Won, J. Moon, J. Choi, S. Kim, The high capacity and cycle stability of NiFe₂O₄ thin film prepared by E-beam evaporation method for lithium ion batteries. *J. Alloys Compd.* **29**, 802–806 (2017)
57. L.Y. Wang, L.H. Zhuo, H.Y. Cheng, C. Zhang, F.Y. Zhao, Porous carbon nanotubes decorated with nanosized cobalt ferrite as anode materials for high-performance lithium-ion batteries. *J. Power Sources* **283**, 289–299 (2015)
58. M. Fu, Z.Z. Qiu, W. Chen, Y.M. Lin, H.L. Xin, B. Yang, H.S. Fan, C.Z. Zhu, J. Xu, NiFe₂O₄ porous nanorods/graphene composites as high-performance anode materials for lithium-ion batteries. *Electrochim. Acta* **248**, 292–298 (2017)
59. Z.H. Liu, D.D. Guan, Q. Yu, L. Xu, Z.C. Zhuang, T. Zhu, D.Y. Zhao, L. Zhou, L.Q. Mai, Monodisperse and homogeneous SiO_x/C microspheres: a promising high-capacity and durable anode material for lithium-ion batteries. *Energy Storage Mater.* **13**, 112–118 (2018)
60. H.L. Fei, Z.W. Peng, L. Li, Y. Yang, W. Lu, E.L.G. Samuel, X.J. Fan, J.M. Tour, Preparation of carbon-coated iron oxide nanoparticles dispersed on graphene sheets and applications as advanced anode materials for lithium-ion batteries. *Nano Res.* **7**, 502–510 (2014)
61. J. Liang, X.Y. Yu, H. Zhou, H.B. Wu, S.J. Ding, X.W. Lou, Bowl-like SnO₂@carbon hollow particles as an advanced anode material for lithium-ion batteries. *Angew. Chem. Int. Edit.* **53**, 12803–12807 (2014)
62. G.M. Zhou, D.W. Wang, L.C. Yin, N. Li, F. Li, H.M. Cheng, Oxygen bridges between NiO nanosheets and graphene for improvement of lithium storage. *ACS Nano* **6**, 3214–3223 (2012)
63. H. Wu, G. Chan, J.W. Choi, I. Ryu, Y. Yao, M.T. McDowell, S.W. Lee, A. Jackson, Y. Yang, L.B. Hu, Y. Cui, Stable cycling of double-walled silicon nanotube battery anodes through solid–electrolyte interphase control. *Nat. Nanotechnol.* **7**, 310–315 (2012)
64. Y.S. Fu, C.Q. Peng, D.S. Zha, J.W. Zhu, L.L. Zhang, X. Wang, Surface pore-containing NiCo₂O₄ nanobelts with preferred (311) plane supported on reduced graphene oxide: a high-performance anode material for lithium-ion batteries. *Electrochim. Acta* **271**, 137–145 (2018)
65. Y. Li, Y. Bai, C. Wu, J. Qian, G.H. Chen, L. Liu, H. Wang, X.Z. Zhou, F. Wu, Three-dimensional fusiform hierarchical micro/nano Li_{1.2}Ni_{0.2}Mn_{0.6}O₂ with a preferred orientation (110) plane as a high energy cathode material for lithium-ion batteries. *J. Mater. Chem. A* **4**, 5942–5951 (2016)

Publisher's Note Springer Nature remains neutral with regard to jurisdictional claims in published maps and institutional affiliations.